

# Effective Sample Pair Generation for Ultrasound Video Contrastive Representation Learning

Yixiong Chen<sup>1,\*</sup>, Chunhui Zhang<sup>2,\*</sup>, Li Liu<sup>3,(✉)</sup>,  
Cheng Feng<sup>4,5</sup>, Changfeng Dong<sup>4,5</sup>, Yongfang Luo<sup>4,5</sup>, Xiang Wan<sup>3</sup>

<sup>1</sup>School of Data Science, Fudan university, Shanghai, China

<sup>2</sup>Institute of Information Engineering, Chinese Academy of Sciences, Beijing, China

<sup>3</sup>Shenzhen Research Institute of Big Data, The Chinese University of Hong Kong Shenzhen, Shenzhen, China

<sup>4</sup>Shenzhen Third People’s Hospital, Shenzhen, China

<sup>5</sup>Southern University of Science and Technology, Shenzhen, China

## Abstract

Most deep neural networks (DNNs) based ultrasound (US) medical image analysis models use pretrained backbones (e.g., ImageNet) for better model generalization. However, the domain gap between natural and medical images causes an inevitable performance bottleneck when applying to US image analysis. Our idea is to pretrain DNNs on US images directly to avoid this bottleneck. Due to the lack of annotated large-scale datasets of US images, we first construct a new large-scale US video-based image dataset named US-4, containing over 23,000 high resolution images from four US video sub-datasets, where two sub-datasets are newly collected by our local experienced doctors. To make full use of this dataset, we then innovatively propose an US semi-supervised contrastive learning (USCL) method to effectively learn feature representations of US images, with a new sample pair generation (SPG) scheme to tackle the problem that US images extracted from videos have high similarities. Moreover, the USCL treats contrastive loss as a consistent regularization, which boosts the performance of pretrained backbones by combining the supervised loss in a mutually reinforcing way. Extensive experiments on down-stream tasks’ fine-tuning show the superiority of our approach against ImageNet pretraining and pretraining using previous state-of-the-art semi-supervised learning approaches. In particular, our pretrained backbone gets fine-tuning accuracy of over 94%, which is 9% higher than 85% of the ImageNet pretrained model on the widely used POCUS dataset. The constructed US-4 dataset and source codes of this work will be made public.

\*The first two authors contributed equally. Work done while at SRIBD. Li Liu is the corresponding author: liuli@cuhk.edu.cn. Project page: <https://github.com/983632847/USCL>

## 1. Introduction

Due to the low cost and portability, ultrasound (US) is one of the most widely used medical imaging techniques, leading to the widespread use of US images [5, 46, 34] for clinical diagnosis. To date, the most popular automatic US image analysis technique is deep neural networks (DNNs) with pretraining [18, 47]. When training DNN on US images, a big challenge is the data scarcity, which is often dealt with parameter transferred from pretrained models (e.g., ImageNet [42]). However, model performance suffers severely from the domain discrepancy between *natural* and *medical* images. The reason why there is no well-pretrained models especially for US images is also the data scarcity, which is due to the high cost of specialized annotations, inconsistent labeling criterion and large diversity of medical image modalities (e.g., CT [23], MRI [14], X-Ray [57] and US [1]).

To address this problem, we first build a large-scale US video dataset<sup>1</sup> to alleviate data shortage. Secondly, since the contrastive learning shows high performance on representation learning [16, 7, 19], we propose to exploit semi-supervised contrastive learning to boost the pretraining performance. However, given the fact that most US data are in video format, if we follow the normal procedure [7, 16], (i.e., extracting frames from videos, and considering two samples augmented from each image as positive pairs, samples from different images as negative pairs), high similarities between negative pairs sampled from the same video will destroy the contrastive training. We call this phenomenon *similarity conflict* in this work. Thus, can we find a way to avoid similarity conflict of contrastive learning and

<sup>1</sup>It should be mentioned that our US dataset is regarded as a large-scale dataset (over 23,000 US images) in medical imaging field, but its amount is still far less than the natural image datasets such as ImageNet (over 14 million images).

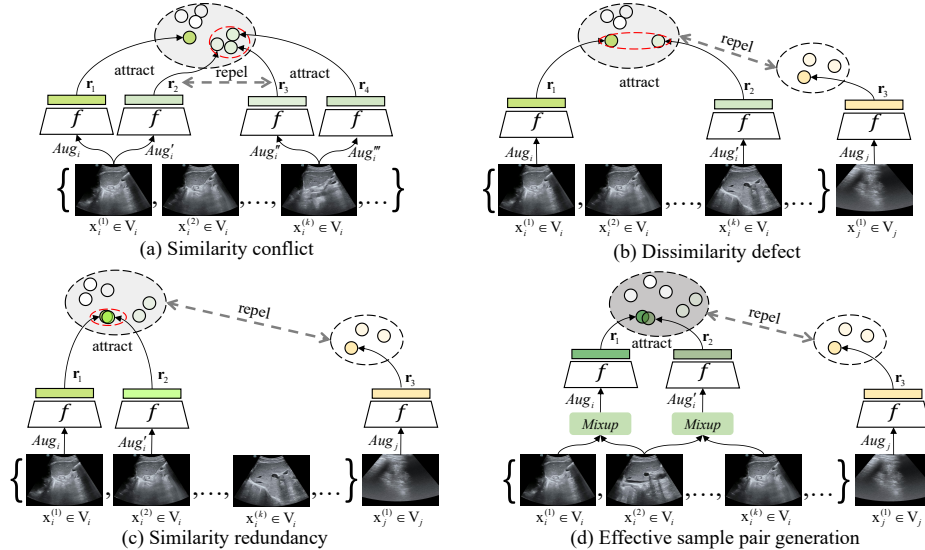


Figure 1. Motivation of our ultrasound contrastive learning approach. (a) Similarity conflict: in traditional contrastive learning, if a negative sample pair comes from a video, their similarity will be higher than that between two augmented positive samples, which confuses the training. (b) Dissimilarity defect: if we sample two frames from a video randomly as a positive pair, they would be too dissimilar if far in temporal. (c) Similarity redundancy: if we sample two frames from a video as a positive pair, they may be too similar if close in temporal. (d) SPG ensures positive pairs to have medium similarity, and negative pairs from different videos to have large dissimilarity. Representations are learned by bringing positive pairs to close in representation space and pushing negative pairs apart.

*train a robust DNN backbone with US videos?*

To answer this question, we find that image features from the same US video can be seen as one cluster in representation space, while features of images from different videos are far away. Thus, randomly extracting two images as a positive pair from each video and regarding two images extracted from different videos as a negative pair is a feasible choice to avoid similarity conflict. However, with this simple process, the situation that two positive samples are too similar or too dissimilar may decrease the training efficiency. In this work, these two problems are called similarity redundancy and dissimilarity defect (see Fig. 1), respectively. To tackle these problems, we innovatively propose an effective sample pair generation (SPG) strategy, which generates a positive pair from a video semantic cluster to control their similarity instead of extracting two frames randomly.

Combined with the SPG, a semi-supervised contrastive learning framework is developed to train a generic pre-train model for US image analysis with standard US videos. Here, we call our whole framework as *ultrasound contrastive learning (USCL)*, which combines supervised learning to ensure the basic pretraining performance, and self-supervised contrastive learning to boost the model discriminative ability. Together with the SPG strategy, USCL makes full use of the implicit structure information of the video-based US image dataset. The overview of our framework is shown in Fig. 4, which contains effective sample generation and semi-supervised contrastive learning.

Experimental results on different target datasets show the superior performance of the proposed method.

The main contributions of this paper are three folds:

- 1) We build a large-scale video-based US dataset to solve the problem of US data scarcity, making directly pretraining on US modal to be possible.
- 2) A semi-supervised contrastive representation learning method with effective sample pair generation is proposed for video-based US backbone pretraining. Our method solves similarity conflict, similarity redundancy and dissimilarity defect problems simultaneously.
- 3) Fine-tuning results on classification and detection tasks demonstrate our method outperforms SOTA semi-supervised and self-supervised learning methods on US image representation learning by a large margin.

## 2. Related Work

**Datasets for US Image Analysis** In previous literatures, many US datasets have been constructed to assess medical image analysis tasks, such as lesion recognition [5, 3], classification [11], detection [54] and segmentation [22]. Early US datasets are mainly independent-image-based, like UDIAT-B [54], BUI [41], thyroid US dataset [39], BUSI [1] and fetal US dataset [49]. In addition to independent images, US videos are more ubiquitous in real world, and can show things that a still image cannot, such as blood flow and organ movement. Compared with early independent-image-based datasets, recent video-based US

Table 1. Statistics of the **US-4** dataset containing 4 video-based sub-datasets. The total number of images is 23,231, uniformly sampled from 1051 videos. Most videos contain 10~50 similar images, which ensures the good property of image clusters.

Sub-dataset	Target type	Mean image size (pixels)	Mean frame rate	Categories	Videos	Images
Butterfly [5]	Lung	658×738	23	2	22	1533
CLUST [46]	Liver	434×530	19	5	63	3150
Liver Fibrosis	Liver	600×807	28	5	296	11714
COVID19-LUSMS	Lung	747×747	17	4	670	6834

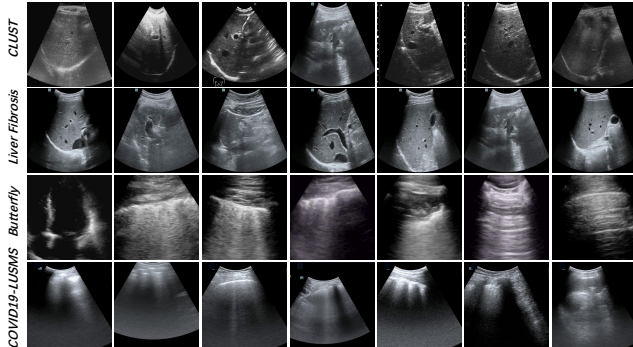


Figure 2. Examples of US image in **US-4**. The newly collected high-quality and well-organized sub-datasets *Liver Fibrosis* and *COVID19-LUSMS* further improve the diversity and effectiveness of the proposed **US-4** dataset.

datasets are becoming much richer [25, 26] and more widely used [46, 30] in automatically clinical diagnostic scenarios. For example, POCUS [32] is a widely used lung video-based US dataset for detecting COVID19.

In [6], a 3D medical segmentation pretraining dataset for CT and MRI was built by aggregating 8 public datasets. Inspired by this, we construct a large-scale labeled video-based US dataset, which is composed of four US sub-datasets containing different organs (*e.g.*, liver and lung). Especially, two sub-datasets with more images are collected and processed by our local doctors. We believe that pre-training on US modal directly with our USCL is able to avoid domain gap and improve representation capability of US analysis models.

**Semi-supervised Learning** This learning scheme aims at complementing supervised learning in unsupervised ways [29, 45] with small amount of labeled samples and rich unlabeled samples. Generally, wrapper methods of inductive semi-supervised learning can be split into three main branches [50], *e.g.*, co-training [4, 37, 28, 40, 12], self-training [31, 52] and boosting [29]. In this work, we focus on a popular sub-field of boosting *i.e.*, consistency regularization (CR) [10], which tries to make DNNs robust to small input perturbations [45]. It was first proposed as “TS” [43] or the “II Model” [29], and a variety of methods aim at generating different kinds of perturbations including data augmentations [51, 13], stochastic regularization

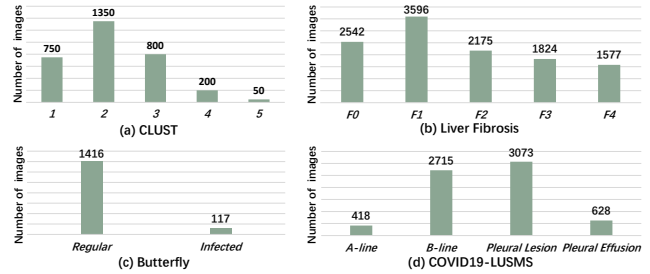


Figure 3. Distribution of the image categories in **US-4**.

[43, 29, 2] and adversarial perturbations [36].

In order to learn more robust visual representations, inspired by the CR paradigm, our approach is designed as a semi-supervised contrastive way. It considers not only a novel form of perturbation (*i.e.*, differences between US video frames), but also includes contrastive learning process for better regularization than the MSE loss in traditional CR.

**Contrastive Learning** The study of contrastive learning dates back to [15], these approaches learn representations by contrasting similar positive sample pairs against dissimilar negative sample pairs. Like CR, contrastive learning wants samples with/without perturbations to be close in feature space, but the differences are that: 1) it can make features from different samples far away from each other; and 2) it can simultaneously make multiple positive samples of an anchor sample close to it and multiple negative samples far away from it [27]. As a branch of self-supervised learning, contrastive learning shows its superiority to other self-supervised works recently [19, 48, 35, 16, 9, 7, 8]. It was shown in [59, 58] that the self-supervised learning methods outperforms ImageNet pretraining on CT and MRI medical imaging analysis because it can effectively exploit large-scale unlabeled data directly. There are works on US image analysis in self-supervised ways [20], but as far as we know, the video-based US frame contrastive learning is still hardly studied [26].

### 3. US-4 Dataset

In this work, we construct a large-scale US dataset named **US-4**, which is collected from four different con-

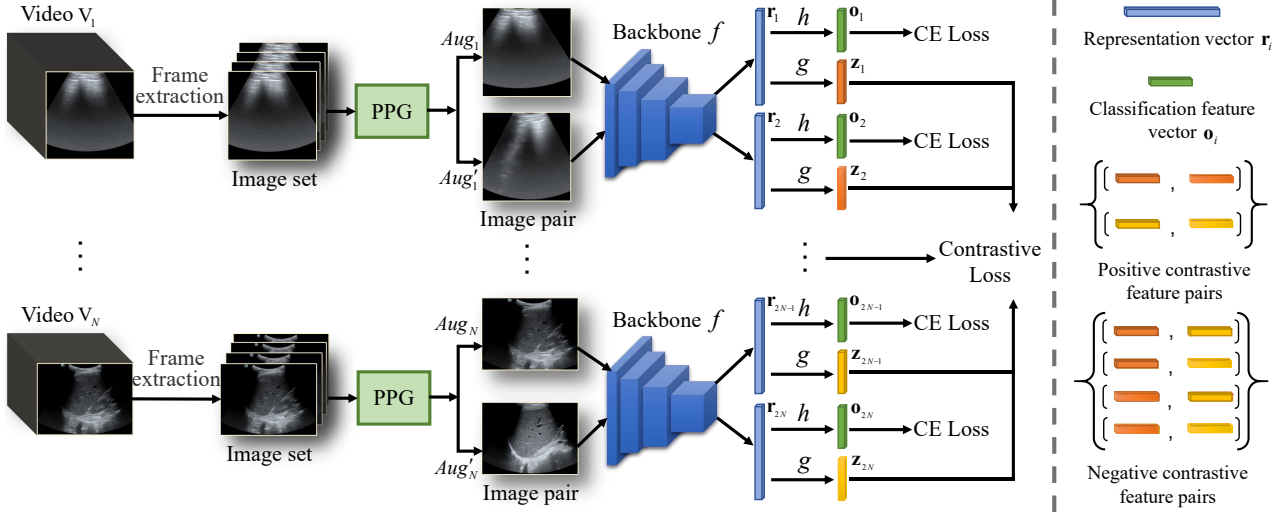


Figure 4. System framework of the proposed USCL, which consists of effective sample pair generation and semi-supervised contrastive learning. (i) We extract evenly distributed image sets from every US video as image dataset. (ii) The positive pair generation (PPG) module consists of a *sampler*  $\Theta$  random sampling several images from a image set, and a *mixed frame generator*  $G$  obtaining two images (Sect. 4.2). These two images from the same video view as a positive pair followed by two separate data augmentation operations. (iii) A base backbone  $f$ , a projection head  $g$  and a classifier  $h$  are trained by simultaneously minimize the self-supervised contrastive learning loss and supervised cross-entropy (CE) loss in multi-task learning fashion (Sect. 4.3).

vex probe [32] US datasets, involving two scan regions (*i.e.*, lung and liver). These sub-datasets contain labeled images captured from videos for classification task. In order to generate a diverse and sufficiently large dataset, images are selected from original videos with a suitable sampling interval. For each raw video with frame rate  $T$ , we extract  $n = 3$  samples per second with sampling interval  $I = \frac{T}{n}$ , which ensures that our US image dataset contains sufficient but not redundant information of videos. This results in our constructed US-4 dataset containing 1051 videos, 23,231 images, which is described in Tab. 1. Fig. 2 shows some examples of our US-4 dataset, and the category distribution of images are shown in Fig. 3. We can see that the US-4 dataset is relatively balanced, where most videos contain tens of US images.

Specifically, *CLUST* sub-dataset [46] contains 63 2D videos, with the number of radiation beams (from one to five) as categories. Each category contains 15, 27, 16, 4 and 1 videos, respectively. *Butterfly* sub-dataset [5] is a lung sub-dataset used to diagnose COVID19, which contains two types of the regular and the infected, with 20 and 2 videos respectively. These two relatively small datasets are open source US datasets. To increase the amount and the diversity of US-4 dataset, we newly collect two US datasets in the local hospital with the help of doctors. The first is *Liver Fibrosis* sub-dataset, which has five categories of F0, F1, F2, F3 and F4, with each category having 71, 93, 53, 42 and 37 videos, respectively. Besides, a multi-symptom lung sub-dataset *COVID19-LUSMS*, which has four classes A-line,

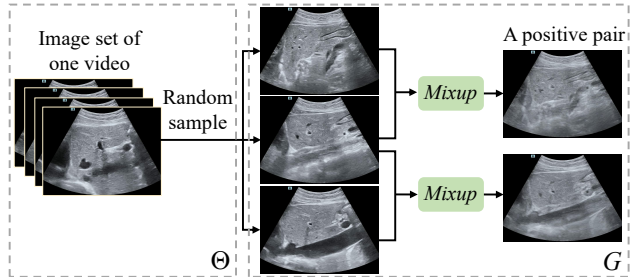


Figure 5. Illustration of the PPG module. It contains two components: a *sampler*  $\Theta$  randomly samples three images from an image set; a *mixed frame generator*  $G$  takes one image as anchor image and uses the mixup operation to generate two new images as a positive pair.

B-line, Pleural Lesion and Pleural Effusion, with 13, 101, 532 and 24 videos, respectively. Though the US-4 is a classification dataset, we will evaluate the generalization and transferability of pretrained models of USCL on US-4 on other tasks, *e.g.*, detection [54] and segmentation [22, 53].

Since four sub-datasets of US-4 are collected by different equipments in different ways, feature space encoded by CNNs can be enriched by different resolutions, clarities and appearances of images. In fact, the difference between data samples is the base of our contrastive training.

## 4. Proposed Method

In this work, our goal is to improve DNN model performance on US image representation learning by the proposed

USCL method (see Fig. 4).

### 4.1. Problem Formulation

Given a video  $V_i$  from US-4 dataset, we first extract images to obtain a balanced distributed frame set  $\mathbb{F}_i^K = \{\mathbf{f}_i^{(k)}\}_{k=1}^K$ , where  $K$  is the number of extracted images. Next, a *sampler*  $\Theta$  is applied to randomly sample  $M$  images, denoted as  $\mathbb{F}_i^M = \{\mathbf{f}_i^{(m)}\}_{m=1}^M$  with  $2 \leq M \ll K$ . Then, we design a *mixed frame generator*  $G : \mathbb{F}_i^M \rightarrow \mathbb{S}_i^2$  to obtain two images, where  $\mathbb{S}_i^2 = \{\mathbf{x}_i^{(1)}, \mathbf{x}_i^{(2)}\}$  is a positive pair followed by two data augmentation operations  $Aug = \{Aug_i, Aug'_i\}$ . These augmentations are used for further perturbing positive pairs, which will be shown in Sect. 4.2 in detail.

The objective of our pretraining framework is to learn a backbone model  $f$  from training samples  $\{(\mathbf{x}_i^{(1)}, \mathbf{x}_i^{(2)}), \mathbf{y}_i\}_{i=1}^N$  by combining self-supervised contrastive learning loss  $\mathcal{L}_{con}$  and supervised cross-entropy loss  $\mathcal{L}_{sup}$ , where  $N$  is the number of videos in a training batch. Therefore, the USCL framework formulation aims to minimize the following loss  $\mathcal{L}$ :

$$\begin{aligned} \mathcal{L} = & \mathcal{L}_{con}(g(f(Aug(G(\mathbf{f})); \mathbf{w}_f); \mathbf{w}_g)) \\ & + \lambda \mathcal{L}_{sup}(h(f(Aug(G(\mathbf{f})); \mathbf{w}_f); \mathbf{w}_h); \mathbf{y}), \end{aligned} \quad (1)$$

where  $\lambda$  is a hyper-parameter,  $\mathbf{f} = \{\{\mathbf{f}_i^{(m)}\}_{m=1}^M\}_{i=1}^N$  are the images randomly sampled from a batch of videos,  $G(\mathbf{f}) = \{\mathbf{x}_i^{(1)}, \mathbf{x}_i^{(2)}\}_{i=1}^N$  are positive pairs, and  $\mathbf{y} = \{\mathbf{y}_i\}_{i=1}^N$  are corresponding class labels.  $f$ ,  $g$  and  $h$  denote base backbone, projection head (will be introduced in Sect. 4.3) and linear classifier, respectively. Different from most existing contrastive learning methods, our framework treats self-supervised contrastive learning loss in Eq. (1) as a CR term, which improves the performance of pretraining backbone by combining supervised loss in a mutually reinforcing way. Here supervised loss constraints the contrastive learning to discriminate better, and contrastive loss regularizes supervised loss to learn more robust representations.

### 4.2. Sample Pair Generation

Most of the existing contrastive learning approaches construct positive pairs by applying two random data augmentations image by image. When directly apply this standard way to the US frames, the contrastive learning fails to work normally due to the similarity conflict problem. To solve this problem, a sample pair generation (SPG) scheme is designed, which includes the process of generating positive and negative sample pairs. To improve the robustness of representation learning, a data augmentation module are then proposed to add more perturbations to the sample pairs.

**Positive Pair Generation Module** The positive pair generation (PPG) module regards an evenly distributed image

set extracted from a video as a cluster, and generates two images as a positive sample pair from this cluster, as shown in Fig. 5. Note that only one positive pair is generated from a video, which can prevent the aforementioned similarity conflict problem (*i.e.*, any negative pair coming from the same video are similar).

In detail, firstly, a *sampler*  $\Theta$  is applied to randomly sample three images  $\widehat{\mathbf{x}}_i^{(1)}, \widehat{\mathbf{x}}_i^{(2)}, \widehat{\mathbf{x}}_i^{(3)}$  in chronological order from an image set  $\{\mathbf{f}_i^{(m)}\}_{m=1}^M$ . Secondly, a delicate *mixed frame generator*  $G$  is performed to generate a positive sample pair. The image  $\widehat{\mathbf{x}}_i^{(2)}$  is set as the anchor image, images  $\widehat{\mathbf{x}}_i^{(1)}$  and  $\widehat{\mathbf{x}}_i^{(3)}$  are perturbation images. In a mini-batch,  $G$  constructs positive sample pairs by the mixup operation [56] between anchor image and two perturbation images as follows.

$$\begin{cases} \mathbf{x}_i^{(1)} = \xi_1 \widehat{\mathbf{x}}_i^{(2)} + (1 - \xi_1) \widehat{\mathbf{x}}_i^{(1)} \\ \mathbf{x}_i^{(2)} = \xi_2 \widehat{\mathbf{x}}_i^{(2)} + (1 - \xi_2) \widehat{\mathbf{x}}_i^{(3)} \\ \mathbf{y}_i^{(1)} = \xi_1 \widehat{\mathbf{y}}_i^{(2)} + (1 - \xi_1) \widehat{\mathbf{y}}_i^{(1)} \\ \mathbf{y}_i^{(2)} = \xi_2 \widehat{\mathbf{y}}_i^{(2)} + (1 - \xi_2) \widehat{\mathbf{y}}_i^{(3)} \end{cases}, \quad (2)$$

where  $\widehat{\mathbf{y}}_i^{(1)}, \widehat{\mathbf{y}}_i^{(2)}$  and  $\widehat{\mathbf{y}}_i^{(3)}$  are corresponding labels,  $\xi_1, \xi_2 \sim Beta(\alpha, \beta)$ , and  $\alpha, \beta$  are parameters of *Beta* distribution.

In our contrastive learning process, two images generated from a video are regarded as a positive pair. These sample pairs are then fed to the backbone followed by the projection head for contrastive learning task. The proposed PPG module has several benefits: 1) positive pairs are random offsets from the anchor image to the perturbation images, which ensures their similarity and reduces the risk of dissimilarity defect; 2) the similarity redundancy of positive pairs is alleviated because a positive pair will only be too similar if  $\{\widehat{\mathbf{x}}_i^{(1)}, \widehat{\mathbf{x}}_i^{(2)}\}$ ,  $\{\widehat{\mathbf{x}}_i^{(2)}, \widehat{\mathbf{x}}_i^{(3)}\}$  are very close simultaneously, which is less likely to happen.

**Negative Pair Generation** The process of generating negative pairs is rather straightforward, we consider any two images generated from different videos in a training batch as a negative pair.

**Data Augmentation Module** The Data Augmentation (DA) Module transforms samples in a mini-batch randomly. This process can be seen as extra perturbation of images, where positive pairs  $\tilde{\mathbf{x}}_i^{(1)} = Aug(\mathbf{x}_i^{(1)})$ , and  $\tilde{\mathbf{x}}_i^{(2)} = Aug'(\mathbf{x}_i^{(2)})$  would get more diverse differences and become harder to distinguish from other negative samples, finally resulting in more robust networks. Here,  $Aug$  contains three simple augmentations: random cropping followed by resizing, random flipping and random color jitter.

### 4.3. Ultrasound Contrastive Learning

The semi-supervised contrastive learning can be seen as a multi-task learning scheme, which learns representations not only by the supervision of category labels, but

---

**Algorithm 1** Backbone learning with USCL

---

**Input:** batch size  $N$ , constant  $\tau$ ,  $\lambda$ , data augmentation  $Aug_i, Aug'_i$ , backbone  $f$ , projection head  $g$ , classifier  $h$ .

**Output:** pretrained backbone  $f$ .

```
1: random initialize  $f, g, h$ 
2: for sampled mini-batch  $\{(\mathbf{x}_i^{(1)}, \mathbf{x}_i^{(2)}), \mathbf{y}_i\}_{i=1}^N$  do
3:   for  $i \in \{1, \dots, N\}$  do
4:     # Augment 2 images generated from a video.
5:      $\tilde{\mathbf{x}}_i^{(1)} = Aug_i(\mathbf{x}_i^{(1)}); \tilde{\mathbf{x}}_i^{(2)} = Aug'_i(\mathbf{x}_i^{(2)})$ 
6:     # Get representations.
7:      $\mathbf{r}_{2i-1} = f(\tilde{\mathbf{x}}_i^{(1)}); \mathbf{r}_{2i} = f(\tilde{\mathbf{x}}_i^{(2)})$ 
8:     # Get outputs from contrast
9:     # and classification branches.
10:     $\mathbf{z}_{2i-1} = g(\tilde{\mathbf{r}}_{2i-1}); \mathbf{z}_{2i} = g(\tilde{\mathbf{r}}_{2i})$ 
11:     $\mathbf{o}_{2i-1} = h(\tilde{\mathbf{r}}_{2i-1}); \mathbf{o}_{2i} = h(\tilde{\mathbf{r}}_{2i})$ 
12:  for  $i \in \{1, \dots, 2N\}$  do
13:    for  $j \in \{1, \dots, 2N\}$  do
14:      # Calculate pairwise similarity.
15:       $s_{i,j} = \mathbf{z}_i \cdot \mathbf{z}_j / (\|\mathbf{z}_i\| \|\mathbf{z}_j\|)$ 
16:      define  $l(i, j) = -\log \frac{\exp(s_{i,j}/\tau)}{\sum_{k=1}^{2N} \mathbb{1}_{i \neq k} \exp(s_{i,k}/\tau)}$ 
17:       $\mathcal{L}_{con} = \frac{1}{2N} \sum_{i=1}^N (l(2i-1, 2i) + l(2i, 2i-1))$ 
18:       $\mathcal{L}_{sup} = \frac{1}{2N} \sum_{i=1}^N (CE(\mathbf{o}_{2i-1}, \mathbf{y}_i) + CE(\mathbf{o}_{2i}, \mathbf{y}_i))$ 
19:       $\mathcal{L} = \mathcal{L}_{con} + \lambda \mathcal{L}_{sup}$ 
20:      update  $f, g, h$  through gradient descent
21: return pretrained  $f$ , discard  $g$  and  $h$ 
```

---

also by maximizing/minimizing agreement between positive/negative pairs as CR. Here, we use ResNet [18] as backbone  $f$  to encode images where the output representation vectors  $\mathbf{r}_{2i-1} = f(\tilde{\mathbf{x}}_i^{(1)})$  and  $\mathbf{r}_{2i} = f(\tilde{\mathbf{x}}_i^{(2)})$  are then fed to the following projection head and classifier. The detailed procedures of our USCL are described in Algorithm 1.

**Contrastive Branch** The contrastive branch consists of a projection head and corresponding contrastive loss. The projection head  $g$  is a two layer MLP which nonlinearly maps representations to other feature space for calculating contrastive regularization loss. The mapped vector  $\mathbf{z}_i = g(\mathbf{r}_i) = \mathbf{w}_g^{(2)} \sigma(\mathbf{w}_g^{(1)} \mathbf{r}_i)$  is specialized for contrast, where  $\sigma$  is ReLU activation function and  $\mathbf{w}_g = \{\mathbf{w}_g^{(1)}, \mathbf{w}_g^{(2)}\}$  are the weights of  $g$ . The contrastive loss is proposed by Sohn [44], which aims at minimizing the distance between positive pairs  $\{\mathbf{x}_i^{(1)}, \mathbf{x}_i^{(2)}\}_{i=1}^N$  and maximizing the distance between any negative pair  $\{\mathbf{x}_i^{(1/2)}, \mathbf{x}_j^{(1/2)}\}, i \neq j$  for CR:

$$\mathcal{L}_{con} = \frac{1}{2N} \sum_{i=1}^N (l(2i-1, 2i) + l(2i, 2i-1)), \quad (3)$$

where

$$l(i, j) = -\log \frac{\exp(s_{i,j}/\tau)}{\sum_{k=1}^{2N} \mathbb{1}_{i \neq k} \cdot \exp(s_{i,k}/\tau)}, \quad (4)$$

and

$$s_{i,j} = \mathbf{z}_i \cdot \mathbf{z}_j / (\|\mathbf{z}_i\| \|\mathbf{z}_j\|), \quad (5)$$

where  $\tau$  is a tuning temperature parameter. As proven by Khosla *et al.* [27], contrastive loss can gain larger  $\|\nabla_{\mathbf{w}} L_{con}\|$  for hard samples pairs. More precisely, for an easy positive pair,  $s_{i,j} \approx 1$ , for an easy negative pair,  $s_{i,j} \approx -1$ , and for any hard pair  $s_{i,j} \approx 0$ . This indicates that the contrastive loss focuses more on hard positives and negatives rather than on simple ones, thus leading to an efficient training. This property is especially important for medical images for which labels are limited.

**Classification Branch** We use a linear classifier  $h$  with weights  $\mathbf{w}_c$  to separate sample features linearly in the representation space similar to [18, 21]. Cross-entropy (CE) loss with corresponding one-hot label  $\mathbf{y}_i$  is

$$\mathcal{L}_{sup} = \frac{1}{2N} \sum_{i=1}^N (CE(\mathbf{o}_{2i-1}, \mathbf{y}_i) + CE(\mathbf{o}_{2i}, \mathbf{y}_i)), \quad (6)$$

where  $\mathbf{o}_i = h(\mathbf{r}_i) = \text{softmax}(\mathbf{w}_c \mathbf{r}_i)$ . Note that traditional CE loss also gains larger gradients when meeting harder samples [24] (*i.e.*, more uniformly distributed feature vector after softmax function instead of one-hot vector), this property makes the classification branch consistent with contrastive branch and improves the learning efficiency.

## 5. Experiment

### 5.1. Experimental Settings

**Network Architecture** In experiments, we use a randomly initialized ResNet-18 [18] as our backbone  $f$ . The feature dimension is reduced to 256 by the last Conv layer. The projection head  $g$  (2 layer MLP) and linear classifier  $h$  (1 fully connected layer) are attached to backbone  $f$  for contrastive learning and classification task, respectively.

**Pretraining Details** We use US-4 dataset for pretraining, and fine-tune pretrained models for various downstream tasks on datasets such as POCUS. During pretraining, US images are randomly cropped and resized to  $224 \times 224$  pixels as our input, followed by random flipping and color jitter. We use Adam optimizer with learning rate  $3 \times 10^{-4}$  and weight decay rate  $10^{-4}$ . The backbone is pretrained on US-4 dataset for 300 epochs with batch size  $N = 32$ , which takes around 1 hour to converge. The pretraining loss is the sum of contrastive loss and standard cross-entropy loss for classification. Like SimCLR [7], the backbone is used for fine-tuning on target tasks, projection head  $g$  and classifier  $h$  are discarded when the pretraining is completed. The  $\lambda$  in Eq. (1) is 0.2, parameters  $\alpha$  and  $\beta$  in Eq. (2) are 0.5 and 0.5, respectively. The temperature parameter  $\tau$  in Eq. (4) is 0.5. Our experiments are implemented using PyTorch [38] with an Intel Xeon Silver 4210R CPU@2.4GHz and a single Nvidia Tesla V100 GPU.

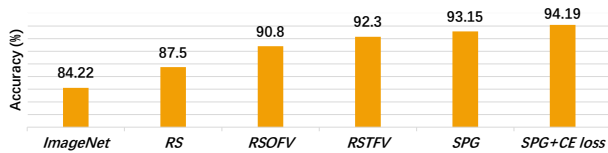


Figure 6. Impact of SPG strategies and CE loss. Our method is pretrained on US-4 and fine-tuned last 3 layers on POCUS.

Table 2. Impact of label rate. Our method is pretrained on US-4 with different label rates and fine-tuned last 3 layers on POCUS.

Label rate (%)	1	10	20	30	40	50
Accuracy (%)	94.19	93.05	90.93	93.67	90.92	92.81

**Fine-tuning Datasets** We fine-tune our pretrained backbones on POCUS, BUSI-BUI joint dataset and UDIAT-B dataset to testify the performance of our USCL. The POCUS [32] is a widely used lung linear probe US dataset for COVID-19 consisting of 140 videos, 2116 images from three classes (*i.e.*, COVID-19, bacterial pneumonia and healthy controls). All fine-tuning results on POCUS are obtained with 5 fold cross validation. The BUSI [1] consists of 780 breast tumor US images with average size of  $500 \times 500$  pixels. These images are categorized into three classes, which are normal, benign and malignant. The BUI [41] contains 250 breast cancer images, 100 benign and 150 malignant. We combine BUSI and BUI datasets together to fine-tune backbones for comparison experiments. Note that images from this joint dataset are collected by linear US probes. Fine-tuning results on BUSI-BUI are also obtained with 5 fold cross validation. The UDIAT-B [55] consists of 163 linear probe US images from different women with a mean image size of  $760 \times 570$  pixels, where each of the images presents one or more lesions. Within the 163 lesion images, 53 are images with cancerous masses and 110 with benign lesions. In this work, we use UDIAT-B dataset to perform the lesion detection and segmentation comparison experiments. 50 of 163 images are used for validation and the rest are used for training.

## 5.2. Ablation Studies

In this section, we report the last-3-layer fine-tuning results on POCUS of US-4 pretrained backbones [32] to validate different components of our approach.

**Sample Pair Generation & CE loss** The impact of different sample pair producing strategies is shown in Fig. 6. ImageNet denotes the ImageNet pretrained backbone as our baseline. We implement four methods using contrastive loss for different sample pair produce strategies, *i.e.*, randomly sample (RS) positive pairs from whole dataset like SimCLR [7], randomly sample one frame (RSOFV) from

Table 3. Impact of batch size. Our method is pretrained on US-4 with different batch sizes and fine-tuned last 3 layers on POCUS.

Batch size	8	16	32	64	128	256
Accuracy (%)	93.10	93.38	94.19	93.76	92.8	91.97

Table 4. Results of pretraining USCL on US-4 with different data groups and fine-tuning last 3 layers on POCUS.

Incremental dataset	Accuracy (%)
Butterfly	84.97
Butterfly+CLUST	88.47
Butterfly+CLUST+Liver Fibrosis	92.01
Butterfly+CLUST+Liver Fibrosis+COVID19-LUSMS	94.19

one video and augment it as a positive pair, randomly sample two frames (RSTFV) from one video as positive, and our SPG. Compared with ImageNet, RS improves the accuracy by 3.28% due to smaller domain gap, RSOFV and RSTFV improve the accuracy by 6.58% and 8.08%, respectively. While the proposed SPG obviously boosts the accuracy by 8.93% (from 84.22% to 93.15%). These results demonstrate the good quality of the proposed SPG.

Moreover, in Fig. 6, we can see that CE loss improves accuracy by 1.04% (from 93.15% to 94.19%). This indicates that extra label information is able to enhance the power of feature representation, which clearly improves the performance of fine-tuning on the target task.

**Impact of Label Rate** The effect of different label rates with our pretrained models is shown in Tab. 2. We train six USCL backbones on US-4 with different label rates. The best accuracy 94.19% is achieved with around 1% labeled data, which is maintained in all our subsequent experiments. We hypothesize that a larger label rate brings less improvement of fine-tuning accuracy because more labeled data increases the risk of overfitting of pretrained models as our training images only come from around 1000 videos.

**Impact of Batch Size** The effect of batch size is shown in Tab. 3. We can see that as the batch size increasing, the accuracy shows a trend from rise to decline, where the best accuracy 94.19% is obtained when batch size is 32. It shows that in our task, bigger batch size (*e.g.*, 4096 in SimCLR [7]) not necessary bring greater gain, because it increases the difficulty of contrastive learning, where the images are limited and have high similarity. To achieve the best trade-off between performance and potential computational cost, we keep batch size as 32 in all our subsequent experiments.

**Pretraining Data Variety** The effect of pretraining data variety is shown in Tab. 4. We can see that when only using *Butterfly* sub-dataset (only 22 videos) as the pretrain, our USCL gets a relatively low last-3-layer fine-tuning accuracy

Table 5. Fine-tuning accuracy (%) on **POCUS dataset**. Our method surpasses all other pretraining methods to a large margin. \* Results of ImageNet and USCL are medium scores w.r.t. “Last 3 layers” selected from 5 times of fine-tuning, respectively.

Pretrain method	Fine-tune scheme		
	Last 1 layer	Last 3 layers	All layers
ImageNet* [18]	85.15	84.22	79.44
US-4 supervised	69.38	85.02	81.19
TE [29]	70.51	81.66	79.4
II Model [29]	73.67	83.18	82.89
FixMatch [45]	70.65	83.6	82.56
MoCo v2 [9]	73.06	84.83	76.28
SimCLR [7]	82.89	86.39	85.87
<b>USCL*</b>	<b>87.85</b>	<b>94.19</b>	<b>86.01</b>

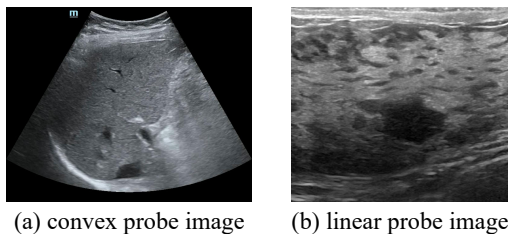


Figure 7. Comparison of convex and linear probe US images.

of 84.97% on POCUS. With the increase of the pretraining sub-datasets, we can see the improvements of the classification accuracy. Especially, when all four sub-datasets are used, the performance is clearly improved by 9.22% (from 84.97% to 94.19%). This shows that the diversity and richness of US-4 dataset is beneficial to our USCL pretraining.

### 5.3. Comparison with SOTA

We use ImageNet pretrained ResNet18 [18] backbone and other seven backbones pretrained on our US-4 dataset with various approaches (*i.e.*, plain supervised, Temporal Ensembling (TE) [29], II Model [29], FixMatch [45], MoCo v2 [9], SimCLR [7] and USCL) for comparison. For supervised or standard semi-supervised methods (*i.e.*, plain supervised, TE, II Model, FixMatch), we consider the dataset as a normal labeled image dataset. For contrastive methods (*i.e.*, MoCo v2, SimCLR, USCL), we only sample negative pairs from different videos for fairness.

**Results on POCUS Classification** On POCUS, linear evaluation is used to testify the representation capability of backbones on target task. We also fine-tune their last 3 layers and all layers to explore the limits of backbones’ capability. Fine-tuning results based on different schemes are shown in Tab. 5. USCL has both the best performance on linear evaluation and multi-layer fine-tuning (87.85% linear evaluation accuracy vs 85.15% for ImageNet pretraining),

Table 6. Fine-tuning accuracy (%) on **BUSI-BUI joint dataset**. \* Results of ImageNet and USCL and medium scores w.r.t. “Last 3 layers” selected from 5 times of fine-tuning, respectively.

Pretrain method	Fine-tune scheme		
	Last 1 layer	Last 3 layers	All layers
ImageNet* [18]	<b>75.38</b>	84.87	81.92
US-4 supervised	62.14	71.26	68.93
TE [29]	61.54	71.84	68.74
II Model [29]	62.91	69.71	66.99
FixMatch [45]	61.65	70.29	72.14
MoCo v2 [9]	63.30	77.77	76.21
SimCLR [7]	69.61	83.11	74.56
<b>USCL*</b>	73.8	<b>85.53</b>	<b>83.11</b>

and its highest accuracy 94.19% is also significantly better than all 7 counterparts. In this experiment, we find that vanilla supervised pretraining cannot achieve better performance than ImageNet pretraining, which indicates the high performance of USCL not only depends on the US-4 dataset, but also depends on its own delicate design.

In addition, contrastive learning based methods (MoCo v2, SimCLR, USCL) noticeably surpass methods that mainly use label supervision (*i.e.*, vanilla supervised learning, TE, II Model, FixMatch). We summarize possible reasons as follows: 1) Though our dataset contains over 20,000 US images, they can be regarded as coming from about 1,000 samples as high similarity, which is not enough for supervised learning method to gain good generalization; 2) The label information of US modal is weak compared with natural images. Moreover, noisy labels and semantically ambiguous samples are common, which further weakens supervised training; 3) The effective features of US are weak compared with background signals, making detail features harder to learn, while contrastive learning can do this better than supervised learning; 4) All labels are available during pretraining, so common semi-supervised methods do not have obviously advantage compared with supervised learning methods.

**Results on BUSI-BUI Classification** Fine-tuning results on BUSI-BUI are shown in Tab. 6. We find that our USCL does not show significant superiority to the ImageNet unlike in POCUS experiment. We hypothesize that it is due to the domain gap between convex and linear probe as shown in Fig. 7. While USCL outperforms all other SOTA methods pretrained on US-4, even their overall accuracy drops compared with ImageNet pretraining. This fact indicates that USCL still works efficiently, but domain gap damages performance of all convex probe data pretrained backbones after transferred to linear probe US images.

**Results on UDIAT-B Detection and Segmentation** In this experiment of detection and segmentation on UDIAT-B dataset, we use Mask R-CNN [17] model and ResNet18-



Table 7. Detection and Segmentation results on **UDIAT-B dataset** under MS COCO metrics. Results for all 8 models are medium scores w.r.t “*detection AP*” selected from 5 times of experiments.

Pretrain method	Lesion detection			Instance segmentation		
	<i>AP</i>	<i>AP</i> <sub>50</sub>	<i>AP</i> <sub>75</sub>	<i>AP</i>	<i>AP</i> <sub>50</sub>	<i>AP</i> <sub>75</sub>
ImageNet [18]	40.6	80.9	40.0	48.2	81.4	51.9
US-4 supervised	38.3	74.2	31.2	42.6	72.1	43.4
TE [29]	38.7	80.8	35.3	46.6	77.8	52.2
II Model [29]	36.1	75.9	29.4	45.5	75.9	54.4
FixMatch [45]	39.6	76.9	31.4	46.9	76.9	55.1
MoCo v2 [9]	38.7	75.5	29.3	47.1	75.4	59.4
SimCLR [7]	43.8	82.3	39.2	<b>51.3</b>	80.5	57.9
<b>USCL</b>	<b>45.4</b>	<b>82.8</b>	<b>40.1</b>	50.7	<b>84.0</b>	<b>61.7</b>

FPNs [33], whose ResNet parts are pretrained on US-4 dataset, the results are shown in Tab 7. We find that SimCLR and USCL get above 45 AP scores in detection task, while ImageNet pretraining only has about 40. In addition, our USCL performs the best when segmentation threshold is relatively low. USCL has higher *AP*<sub>50</sub> and *AP*<sub>75</sub> in segmentation task, showing better correctness of the predicted masks, which is important for clinical diagnosis. Importantly, in both detection and segmentation task, USCL and SimCLR outperform the ImageNet pretraining by a large margin in spite of convex-linear domain gap, showing that contrastive pretraining works well in grasping detail information of images than vanilla supervised pretraining.

## 6. Conclusion

In this work, we construct an US video-based image dataset and propose an efficient contrastive semi-supervised learning algorithm (*i.e.*, USCL) for US image pretraining. Our method conducts contrastive and supervised learning simultaneously to learn robust representations, where SPG avoids problems of sample pair similarity and makes contrastive process work efficiently. Experiments show that our method greatly outperforms ImageNet pretraining and previous SOTA approaches on different US image analysis tasks. In the future, we will add more diverse data to bridge the domain gap between convex and linear probes, and investigate how to use more types of US images (*e.g.*, independent US images) for pretraining.

## References

[1] Walid Al-Dhabyani, Mohammed Gomaa, Hussien Khaled, and Aly Fahmy. Dataset of breast ultrasound images. *Data in Brief*, 28, 11 2019. 1, 2, 7

[2] Philip Bachman, Ouais Alsharif, and Doina Precup. Learning with pseudo-ensembles. In *NeurIPS*, pages 3365–3373, 2014. 3

[3] Adrien Besson, Dimitris Perdios, Florian Martinez, Zhouye Chen, Rafael E Carrillo, Marcel Arditi, Yves Wiaux, and

Jean-Philippe Thiran. Ultrafast ultrasound imaging as an inverse problem: Matrix-free sparse image reconstruction. *IEEE transactions on ultrasonics, ferroelectrics, and frequency control*, 65(3):339–355, 2017. 2

[4] Avrim Blum and Tom Mitchell. Combining labeled and unlabeled data with co-training. In *COLT*, pages 92–100, 1998. 3

[5] Jannis Born, Gabriel Brändle, Manuel Cossio, Marion Disdier, Julie Goulet, Jérémie Roulin, and Nina Wiedemann. Pocus-net: automatic detection of covid-19 from a new lung ultrasound imaging dataset (pocus). *arXiv:2004.12084*, 2020. 1, 2, 3, 4

[6] Sihong Chen, Kai Ma, and Yefeng Zheng. Med3d: Transfer learning for 3d medical image analysis. *arXiv:1904.00625*, 2019. 3

[7] Ting Chen, Simon Kornblith, Mohammad Norouzi, and Geoffrey Hinton. A simple framework for contrastive learning of visual representations. *arXiv:2002.05709*, 2020. 1, 3, 6, 7, 8, 9

[8] Ting Chen, Simon Kornblith, Kevin Swersky, Mohammad Norouzi, and Geoffrey Hinton. Big self-supervised models are strong semi-supervised learners. *arXiv:2006.10029*, 2020. 3

[9] Xinlei Chen, Haoqi Fan, Ross Girshick, and Kaiming He. Improved baselines with momentum contrastive learning. *arXiv:2003.04297*, 2020. 3, 8, 9

[10] Veronika Cheplygina, Marleen de Bruijne, and Josien PW Pluim. Not-so-supervised: a survey of semi-supervised, multi-instance, and transfer learning in medical image analysis. *Medical image analysis*, 54:280–296, 2019. 3

[11] Jianning Chi, Ekta Walia, Paul Babyn, and *et al.* Thyroid nodule classification in ultrasound images by fine-tuning deep convolutional neural network. *Journal of digital imaging*, 30(4):477–486, 2017. 2

[12] WeiWang Dong-DongChen and Zhi-HuaZhou WeiGao. Tri-net for semi-supervised deep learning. In *IJCAI*, pages 2014–2020, 2018. 3

[13] Geoffrey French, Michal Mackiewicz, and Mark Fisher. Self-ensembling for visual domain adaptation. *arXiv:1706.05208*, 2017. 3

[14] Zaiwang Gu, Jun Cheng, Huazhu Fu, Kang Zhou, Huaying Hao, Yitian Zhao, Tianyang Zhang, Shenghua Gao, and Jiang Liu. Ce-net: Context encoder network for 2d medical image segmentation. *TMI*, 38(10):2281–2292, 2019. 1

[15] Raia Hadsell, Sumit Chopra, and Yann LeCun. Dimensionality reduction by learning an invariant mapping. In *CVPR*, volume 2, pages 1735–1742, 2006. 3

[16] Kaiming He, Haoqi Fan, Yuxin Wu, Saining Xie, and Ross Girshick. Momentum contrast for unsupervised visual representation learning. In *CVPR*, pages 9729–9738, 2020. 1, 3

[17] Kaiming He, Georgia Gkioxari, Piotr Dollár, and Ross B. Girshick. Mask r-cnn. *TPAMI*, 2020. 8

[18] Kaiming He, Xiangyu Zhang, Shaoqing Ren, and Jian Sun. Deep residual learning for image recognition. In *CVPR*, pages 770–778, 2016. 1, 6, 8, 9

- [19] Olivier J Hénaff, Aravind Srinivas, Jeffrey De Fauw, Ali Razavi, Carl Doersch, SM Eslami, and Aaron van den Oord. Data-efficient image recognition with contrastive predictive coding. *arXiv:1905.09272*, 2019. 1, 3
- [20] Szu-Yen Hu, Shuhang Wang, Wei-Hung Weng, JingChao Wang, XiaoHong Wang, Arinc Ozturk, Quan Li, Viksit Kumar, and Anthony E Samir. Self-supervised pretraining with dicom metadata in ultrasound imaging. In *Machine Learning for Healthcare Conference*, pages 732–749, 2020. 3
- [21] Gao Huang, Zhuang Liu, Laurens Van Der Maaten, and Kilian Q Weinberger. Densely connected convolutional networks. In *CVPR*, pages 4700–4708, 2017. 6
- [22] Qinghua Huang, Yaozhong Luo, and Qiangzhi Zhang. Breast ultrasound image segmentation: a survey. *International journal of computer assisted radiology and surgery*, 12(3):493–507, 2017. 2, 4
- [23] Jeremy Irvin, Pranav Rajpurkar, and Michael Ko. Chexpert: A large chest radiograph dataset with uncertainty labels and expert comparison. In *AAAI*, pages 590–597, 2019. 1
- [24] Katarzyna Janocha and W. Czarnecki. On loss functions for deep neural networks in classification. In *TFML*, 2017. 6
- [25] Jianbo Jiao, Yifan Cai, Mohammad Alsharid, Lior Drukker, Aris T.Papageorghiou, and J. Alison Noble. Self-supervised contrastive video-speech representation learning for ultrasound. In *MICCAI*, 2020. 3
- [26] Jianbo Jiao, Richard Droste, Lior Drukker, Aris T Papageorghiou, and J Alison Noble. Self-supervised representation learning for ultrasound video. In *ISBI*, pages 1847–1850, 2020. 3
- [27] Prannay Khosla, Piotr Teterwak, Chen Wang, Aaron Sarna, Yonglong Tian, Phillip Isola, Aaron Maschiot, Ce Liu, and Dilip Krishnan. Supervised contrastive learning. *arXiv:2004.11362*, 2020. 3, 6
- [28] Abhishek Kumar and Hal Daumé. A co-training approach for multi-view spectral clustering. In *ICML*, pages 393–400, 2011. 3
- [29] Samuli Laine and Timo Aila. Temporal ensembling for semi-supervised learning. In *ICLR*, 2017. 3, 8, 9
- [30] S. Leclerc, E. Smistad, J. Pedrosa, A. Østvik, F. Cervnansky, F. Espinosa, T. Espeland, E. A. R. Berg, P. M. Jodoin, T. Grenier, C. Lartizien, J. D’hooge, L. Lovstakken, and O. Bernard. Deep learning for segmentation using an open large-scale dataset in 2d echocardiography. *TMI*, 38(9):2198–2210, 2019. 3
- [31] Dong-Hyun Lee. Pseudo-label: The simple and efficient semi-supervised learning method for deep neural networks. In *ICML Workshop*, volume 3, 2013. 3
- [32] D.-H. Lee. c-net: Automatic detection of covid-19 from a new lung ultrasound imaging dataset (pocus). *arXiv*, 2020. 3, 4, 7
- [33] Tsung-Yi Lin, Piotr Dollár, Ross Girshick, Kaiming He, Bharath Hariharan, and Serge Belongie. Feature pyramid networks for object detection. In *CVPR*, 2017. 9
- [34] Thomas P Matthews, Kun Wang, Cuiping Li, Neb Duric, and Mark A Anastasio. Regularized dual averaging image reconstruction for full-wave ultrasound computed tomography. *IEEE transactions on ultrasonics, ferroelectrics, and frequency control*, 64(5):811–825, 2017. 1
- [35] Ishan Misra and Laurens van der Maaten. Self-supervised learning of pretext-invariant representations. In *CVPR*, pages 6707–6717, 2020. 3
- [36] Takeru Miyato, Shin-ichi Maeda, Masanori Koyama, and Shin Ishii. Virtual adversarial training: a regularization method for supervised and semi-supervised learning. *TPAMI*, 41(8):1979–1993, 2018. 3
- [37] Kamal Nigam and Rayid Ghani. Analyzing the effectiveness and applicability of co-training. In *CIKM*, pages 86–93, 2000. 3
- [38] Adam Paszke, Sam Gross, Francisco Massa, Adam Lerer, and Soumith Chintala. Pytorch: An imperative style, high-performance deep learning library. 2019. 6
- [39] Lina Pedraza, Carlos Vargas, Fabián Narváez, Oscar Durán, Emma Muñoz, and Eduardo Romero. An open access thyroid ultrasound image database. In *SPIE*, volume 9287, 2015. 2
- [40] Siyuan Qiao, Wei Shen, Zhishuai Zhang, Bo Wang, and Alan Yuille. Deep co-training for semi-supervised image recognition. In *ECCV*, pages 135–152, 2018. 3
- [41] Paulo Sergio Rodrigues. Breast ultrasound image. *Mendeley Data*, VI, doi: 10.17632/wmy84gzngw.1, 2018. 2, 7
- [42] Olga Russakovsky, Jia Deng, Hao Su, and *et al.* ImageNet Large Scale Visual Recognition Challenge. *IJCV*, 115(3):211–252, 2015. 1
- [43] Mehdi Sajjadi, Mehran Javanmardi, and Tolga Tasdizen. Regularization with stochastic transformations and perturbations for deep semi-supervised learning. In *NeurIPS*, pages 1163–1171, 2016. 3
- [44] Kihyuk Sohn. Improved deep metric learning with multi-class n-pair loss objective. In *NeurIPS*, pages 1857–1865, 2016. 6
- [45] Kihyuk Sohn, David Berthelot, Chun-Liang Li, and *et al.* Fixmatch: Simplifying semi-supervised learning with consistency and confidence. *arXiv:2001.07685*, 2020. 3, 8, 9
- [46] O. Somphone, S. Allaire, B. Mory, and C. Dufour. Live feature tracking in ultrasound liver sequences with sparse demons. In *MICCAI Workshop*, pages 53–60, 2014. 1, 3, 4
- [47] Nima Tajbakhsh, Jae Y Shin, Suryakanth R Gurudu, R Todd Hurst, Christopher B Kendall, Michael B Gotway, and Jianming Liang. Convolutional neural networks for medical image analysis: Full training or fine tuning? *TMI*, 35(5):1299–1312, 2016. 1
- [48] Yonglong Tian, Dilip Krishnan, and Phillip Isola. Contrastive multiview coding. *arXiv:1906.05849*, 2019. 3
- [49] Thomas LA van den Heuvel, Dagmar de Bruijn, Chris L de Korte, and Bram van Ginneken. Automated measurement of fetal head circumference using 2d ultrasound images. *PloS one*, 13(8), 2018. 2
- [50] Jesper E Van Engelen and Holger H Hoos. A survey on semi-supervised learning. *Machine Learning*, 109(2):373–440, 2020. 3
- [51] Qizhe Xie, Zihang Dai, Eduard Hovy, Minh-Thang Luong, and Quoc V Le. Unsupervised data augmentation for consistency training. *arXiv:1904.12848*, 2019. 3

- [52] Qizhe Xie, Minh-Thang Luong, Eduard Hovy, and Quoc V Le. Self-training with noisy student improves imagenet classification. In *CVPR*, pages 10687–10698, 2020. [3](#)
- [53] Yuan Xu, Yuxin Wang, Jie Yuan, and *et al.* Medical breast ultrasound image segmentation by machine learning. *Ultrasonics*, 91:1–9, 2019. [4](#)
- [54] Moi Hoon Yap, Gerard Pons, Joan Martí, and *et al.* Automated breast ultrasound lesions detection using convolutional neural networks. *IEEE J BIOMED HEALTH*, 22(4):1218–1226, 2017. [2](#), [4](#)
- [55] Moi Hoon Yap, Gerard Pons, Joan Martí, and *et al.* Automated breast ultrasound lesions detection using convolutional neural networks. *JBHI*, 22(4):1218–1226, 2017. [7](#)
- [56] Hongyi Zhang, Moustapha Cisse, Yann N. Dauphin, and David Lopez-Paz. mixup: Beyond empirical risk minimization. In *ICLR*, 2018. [5](#)
- [57] Hong Yu Zhou, Shuang Yu, Cheng Bian, Yifan Hu, Kai Ma, and Yefeng Zheng. Comparing to learn: Surpassing imagenet pretraining on radiographs by comparing image representations. In *MICCAI*, 2020. [1](#)
- [58] Hong-Yu Zhou, Shuang Yu, Cheng Bian, Yifan Hu, Kai Ma, and Yefeng Zheng. Comparing to learn: Surpassing imagenet pretraining on radiographs by comparing image representations. In *MICCAI*, pages 398–407, 2020. [3](#)
- [59] Zongwei Zhou, Vatsal Sodha, Md Mahfuzur Rahman Siddiquee, and *et al.* Models genesis: Generic autodidactic models for 3d medical image analysis. In *MICCAI*, pages 384–393, 2019. [3](#)